

Article

Magnetic Carbon Nanofiber Mats for Prospective Single Photon Avalanche Diode (SPAD) Sensing Applications

Marah Trabelsi ¹, Al Mamun ², Michaela Klöcker ³, Imane Moulefera ⁴, Anton Pljonkin ⁵ , Khaled Elleuch ¹ 
and Lilia Sabantina ^{2,*} 

¹ Ecole Nationale d'Ingénieurs de Sfax, Laboratory LGME, University of Sfax, Sfax 3038, Tunisia; marah.trabelsi@enis.tn (M.T.); khaled.elleuch@enis.tn (K.E.)

² Junior Research Group "Nanomaterials", Faculty of Engineering and Mathematics, Bielefeld University of Applied Sciences, 33619 Bielefeld, Germany; al.mamun@fh-bielefeld.de

³ Faculty of Engineering and Mathematics, Bielefeld University of Applied Sciences, 33619 Bielefeld, Germany; michaela.kloecker@fh-bielefeld.de

⁴ L.M.A.E. Laboratory, Department of Process Engineering, Faculty of Science and Technology, University of Mustapha Stambouli, Mascara 29000, Algeria; imanemoulefera@yahoo.fr

⁵ Institute of Computer Technology and Information Security, Southern Federal University (SFedU), 347900 Taganrog, Russia; pljonkin@mail.ru

* Correspondence: lilia.sabantina@fh-bielefeld.de

Abstract: Electrospinning enables simple and cost-effective production of magnetic nanofibers by adding nanoparticles to a polymer solution. In order to increase the electrical conductivity of such nanofibers, the carbonization process is crucial. In this study, the chemical and morphological properties of magnetic nanofiber mats prepared from polyacrylonitrile (PAN)/magnetite were investigated. In our previous studies, PAN/magnetite nanofiber mats were carbonized at 500 °C, 600 °C, and 800 °C. Here, PAN/magnetite nanofiber mats were carbonized at 1000 °C. The surface morphology of these PAN/magnetite nanofiber mats is not significantly different from nanofiber mats thermally treated at 800 °C and have remained relatively flexible at 1000 °C, which can be advantageous for various application fields. The addition of nanoparticles increased the average fiber diameter compared to pure PAN nanofiber mats and improved the dimensional stability during thermal processes. The high conductivity, the high magnetization properties, as well as shielding against electromagnetic interference of such carbonized nanofibers can be proposed for use in single photon avalanche diode (SPAD), where these properties are advantageous.

Keywords: carbon nanofibers; carbonization; magnetic nanoparticles; magnetite; PAN



Citation: Trabelsi, M.; Mamun, A.; Klöcker, M.; Moulefera, I.; Pljonkin, A.; Elleuch, K.; Sabantina, L. Magnetic Carbon Nanofiber Mats for Prospective Single Photon Avalanche Diode (SPAD) Sensing Applications. *Sensors* **2021**, *21*, 7873. <https://doi.org/10.3390/s21237873>

Academic Editor: Erika Scavetta

Received: 27 September 2021

Accepted: 19 November 2021

Published: 26 November 2021

Publisher's Note: MDPI stays neutral with regard to jurisdictional claims in published maps and institutional affiliations.



Copyright: © 2021 by the authors. Licensee MDPI, Basel, Switzerland. This article is an open access article distributed under the terms and conditions of the Creative Commons Attribution (CC BY) license (<https://creativecommons.org/licenses/by/4.0/>).

1. Introduction

Magnetic nanofibers are produced by introducing magnetic nanoparticles into a polymer solution using an electrospinning process, which is simple and cost-effective [1–3]. Due to their high surface-to-volume ratio and high porosity, nanofibers have excellent sensitivity and high sensing performance, which makes them attractive for sensing applications such as detection of various gases, strain sensors, etc., [4,5]. Electrospinning is a very efficient and versatile method for manufacturing nanofibers on a large scale and at low cost [6–8]. In general, all electrospinning techniques are based on the following procedure: polymer is dissolved in a solvent and this polymer solution or melt is introduced into an electric field. By applying a high voltage between two electrodes, Taylor cones are simultaneously formed and result in ultrathin nanoscale fibers, which are deposited on the substrate [9,10]. In general, needle-based and needle-free electrospinning techniques are often used. With needle-free electrospinning technology, on which the Nanospider[®] electrospinning machine (Elmarco s.r.o., Liberec, Czech Republic) is based, it is possible to produce relatively large quantities of nanofibers in the same quality. The schematic layout of the Nanospider[®] Lab machine is shown in Figure 1.

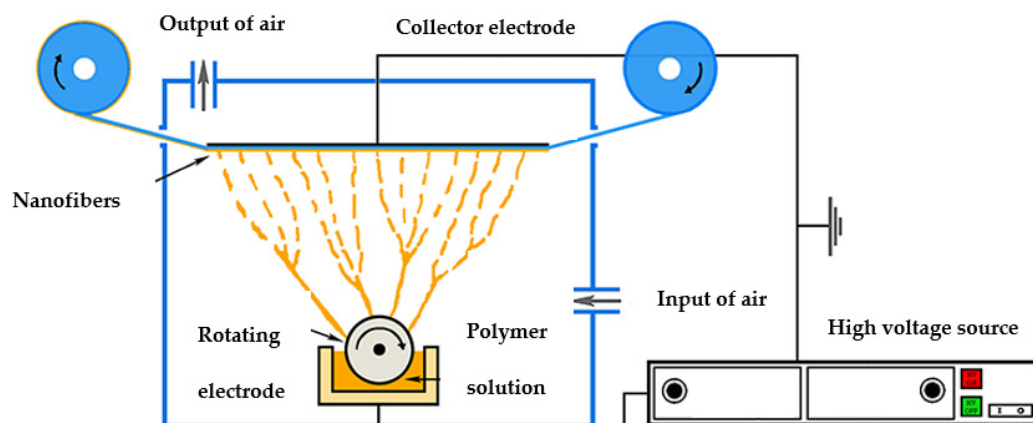


Figure 1. Schematic of the needle-less electrospinning setup. Adapted with permission from reference [11], Sasithorn et al., 2016, originally published under a CC-BY 3.0 license.

Polyacrylonitrile (PAN) polymer is often used to prepare nanofiber mats [12] as it exhibits water-resistant properties and is applicable in many defined areas requiring this property, such as water purification, filtration, or medical areas [13,14]. In addition, PAN is often used for the production of carbon nanofibers, as it is known to have a high carbon yield [15,16]. Carbon nanofibers exhibit high electrical conductivity, low density, as well as high specific strength. Moreover, carbon nanofiber mats are easy to handle and overcome all major challenges in dispersion, processing, and handling compared to other carbon nanomaterials such as carbon nanotubes [17–20].

Magnetic nanofibers are of great interest for basic research of their magnetic properties as well as for possible applications in spintronics, neuromorphic computing and data transfer [21–23]. Secure data transfer is of great interest nowadays and requires effective strategies [24,25]. For some kinds of applications, nanofiber mats with agglomeration and beads are advantageous because magnetic nanoparticles collect in beads and thus form a network with nodes [2]. Typically, the formation of beads in nanofiber mats is not desired, and various strategies are proposed to avoid the formation of beads, such as the use of surfactants, mechanical mixing or surface modification [26]. Changing the viscosity of the electrospinning solution, changing the amount of polymers, changing the distance between the electrode and the substrate on which the nanofibers accumulate to get the nanofiber mats morphology from nanofiber mats to membrane, mixing the polymer solution by ultrasound etc., are just some of the many other ways to change the nanofiber mats morphology mentioned here [27–30].

The nanofiber mats prepared by electrospinning and carbon nanofiber mats are widely used in the fields of filtration, separation, sensors, catalyst support, energy storage, biomedicine, shielding from radiation, etc., [31–37]. The application of carbon nanofibers in the field of sensing elements is based on their electronic transport properties, which are modulated by the physical-chemical interaction of the sensing element [38]. One-dimensional (1D) nanomaterials, such as nanofibers, contain shortened paths for electron transfer and favor the penetration of electrolyte along the longitudinal axis of nanofibers, which results in improved sensor performance [39].

Many chemoresistive detectors are prepared using electrospinning methods to obtain easy-to-produce micrometer-sized detectors with high sensitivity, increased detection rates, stability, and cross sensitivity [36,40,41]. Ali et al. presented the development of an immunosensor based on mesoporous zinc oxide nanofibers (ZnO-NFs) for breast cancer screening [42]. Chowdhury et al. developed an impedimetric biosensor using polyaniline (PANI) nanofibers that were deposited on a gold (Au) electrode using the cyclic voltammetry technique for the detection of *Escherichia coli* O157:H7 bacteria [43]. Zhang et al. used graphene oxide (GO) nanofibers decorated with nickel oxide (NiO) for the electrochemical detection of glucose [44]. Luo et al. reported a lateral flow immunosensor based on elec-

trospun cellulose nitrate nanofibers and magnetic nanoparticles (γ - Fe_2O_3) to detect *E. coli* O₁₅₇:H₇ colonies [45]. Moreover, Bahrami et al. manufactured a sensitive electrochemical sensor from PVA with iron salts (FeCl_2 : FeCl_3) as magnetic fibers combined with graphite powder and paraffin oil for morphine analysis in biological samples [46]. In addition, magnetic nanofibers are widely used in the field of wires. An electrospun polycarbonate urethane polymer (PCU) with nickel (Ni) was prepared, and its nanostructured wires exhibited high longitudinal elastomagnetic strain and high transverse deflection in response to magnetic field stimuli [47]. The magnetic carbon nanofibers can be used in wastewater treatment. Li et al. successfully synthesized the Fe_3O_4 /PAN-modified magnetic carbon nanofibers (MNFs) by electrospinning and produced horseradish peroxidase-(H-MNFs), which achieved a phenol removal efficiency of 85% the first time and 52% after recycling five times [48]. On the other hand, magnetic nanofibers with core (Fe_3O_4 nanoparticle suspension)/sheath (polyethylene terephthalate) structure were successfully fabricated by electrospinning [49]. The obtained magnetic nanofibers showed superparamagnetic behavior at room temperature as well as favorable mechanical properties, and this leads to many application areas, such as sensors and/or smart bulletproof vests where these magnetic nanofibers can be used [50].

The fact that conductivity increases with increasing carbonization temperature was confirmed in several studies [51,52]. Carbon nanofibers belong to an important class of graphitic materials and are similar in structure in many ways to crystalline three-dimensional graphite. During oxidative stabilization and carbonization processes, the aromatic groups or the groups with ring structure due to the cyclization or crosslinking of the precursor chains lead to aromatization. These processes require the formation of carbon nanofibers with uniform carbon structure and promote electronic mobility, which results in high electrical conductivity [53].

The defined properties and the use of magnetic nanofiber mats were discussed in several studies. In the study by Zuo et al., porous magnetic carbon nanofibers (P-CNF/Fe) were fabricated and absorption of electromagnetic waves was investigated. The minimum reflection coefficient reached -44.86 dB at 4.42 GHz. Moreover, the largest effective absorption bandwidth (EAB) was in the frequency range from 12.96 to 16.24 GHz and reached the value of 3.28, which indicates the approach of such P-CNF/Fe in EM wave attenuation [54]. Fe_3O_4 /carbon composite nanofibers prepared from polyacrylonitrile (PAN)/acetylacetone iron (AAI) and carbonized at 800 °C were evaluated in the study by Zhang et al. for microwave absorption. It was found that adding Fe_3O_4 particles leads to an improvement in electrical conductivity [55]. Bayat et al. investigated the effectiveness of electromagnetic interference (EMI) shielding effectiveness (SE) by multifunctional Fe_3O_4 /carbon nanofibers. The maximum EMI SE of 67.9 dB was obtained [56].

In our previous study by Döpke et al., PAN/magnetite nanofiber mats were prepared and the magnetic properties were investigated [2]. Here, networks of magnetic nanofibers with beads that can be used to transport data in the form of domain walls moving along them and combined with objects that could be used to store data and transport [2–57] are of interest. The use of such fibers is attractive not only for sensing applications but also for other technologies where these properties are advantageous. In a previous study by Fokin et al. [58], magnetic nanofibers were also oxidatively stabilized and carbonized at 500 °C and 800 °C in order to increase the electrical conductivity and enhance stronger contraction and networking of nanofibers to each other, being supportive of magnetic data transmission and other application areas where these properties are beneficial. Usually, when considering scientific literature, different strategies are proposed to avoid agglomeration and beads in nanofibers. In our study and other aforementioned studies, the beads are advantageous because it is assumed that magnetic nanoparticles accumulate there and are crucial for the electrical, magnetic, mechanical, and other properties. In our previous study by Trabelsi et al. [21], PAN/magnetite nanofiber mats were prepared and incipiently carbonized at 500 °C. It was found that visual observation by confocal laser scanning microscopy (CLSM) or scanning electron microscopy (SEM) could not clearly detect agglomerations in the

nanofibers. However, using energy dispersive X spectroscopy (EDS), nanofibers can be easily analyzed to detect agglomerations of magnetic nanoparticles without the use of costly techniques and preparation time such as TEM [21]. The magnetic properties of PAN/magnetite nanofiber mats were investigated on the nanoscale by Weiss and Ehrmann using magnetic force microscopy (MFM) [59], showing less clear differentiation between magnetic and polymeric parts than EDS. The carbonization of PAN/magnetite nanofiber mats at 500 °C, 600 °C, 800 °C, and 1000 °C was carried out by Trabelsi et al. Based on the study mentioned, this study was extended and supplemented [60].

Nanofiber mats and nanofiber mats with magnetic particles can be used in many applications due to their excellent properties such as super capacitance, excellent mechanical properties, and shielding against electromagnetic interference [61,62]. These properties offer a potential application of magnetic carbon nanofiber mats for use in single photon avalanche diodes (SPADs), where high conductivity and high magnetization properties as well as shielding against electromagnetic interference are important to improve the construction design of such sensors.

The SPAD arrays can be considered as solid-state detectors providing imaging capabilities at the single photon level and are used in areas of data and telecommunication security, quantum key distribution applications, advanced driver assistance systems, fluorescence detection, remote-sensing technology, biophotonics, and robotics [63–70]. Advantages of SPADs include unprecedented photon counting and time-resolved performance, and therefore they can be used when deep sub-nanosecond timing performance is required [63,64,68]. On the technological side, the development of high-performance and low-noise SPADs is challenging because many aspects are considered, and compromises have to be made to balance sensitivity against noise and speed against fill factor [70].

The new application areas for optical quantum information and quantum key distribution (QKD) require the rapid developments in detector performance [71–73]. There is a great need for new device concepts that can be used practically for optical quantum information technologies, because the conventional photon counting detectors cannot technically meet all the requirements [74]. New detector technologies are constantly evolving and are highly relevant for many applications such as optical quantum information technologies [75]. Semiconductor detectors, such as SPADs, are used in the fields of quantum optics and quantum information transfer. Currently, some challenges are still observed in the area of secure data transfer. The performance of SPADs is not yet mature enough to ensure secure quantum information such as the distribution of quantum keys over long distances in optical fibers [75].

Most detectors include a probability of recording false counts such as dark current pulses (DCPs), dark counts, or dark noise [76]. These effects are caused by the material properties of the detector, bias conditions, or susceptibility to external noise. Protection from these negative effects will significantly improve the performance of SPADs.

In Figure 2, the novel construction design for the SPAD is presented and the possible use of magnetic nanofibers as a protection against external noise by electromagnetic shielding is proposed in this study and serves as a basis for further development. The nanofibers are expected to reduce dark current pulses (DCPs) generated by external noise. The DCP level is directly related to quantum errors (QBER), and the lower the DCP, the lower the QBER, which is beneficial for the speed of signal transmission.

An avalanche photodiode SPAD is based on Geiger-mode principle, where the electric field of the junction is so strong that even a single charge carrier such as electron or hole causes an avalanche. To restore the original bias state, a passive or active quenching circuit is needed [77].

In the Wang et al. study, electric-field-drive single photon avalanche diode with barrier enhancement was investigated for fluorescence detection [78]. The study by Ejdehakosh et al. deals with the development of new optical random number generator and a simulation with the use of post-layout in 180 nm standard CMOS (complementary metal oxide semiconductor) technology. The circuit was designed using three parallel SPADs

with the aim of detecting photons. To reduce the dark count rate and post-pulsing, one of the three SPADs was biased in Geiger-mode while the other two SPADs were in hold off mode. Here, the SPAD circuit model served to verify the functionality of the circuit [79]. The effect of the electric field on primary dark pulses in SPADs for advanced radiation detection applications was investigated in the study by Lim et al. [80]. The arrays of SPADs include many positive features, such as compactness, high detection efficiency, low operating voltage, magnetic field resistance, rapid time response, and can therefore replace conventional photomultiplier tubes (PMTs) in many radiation detection applications [80].

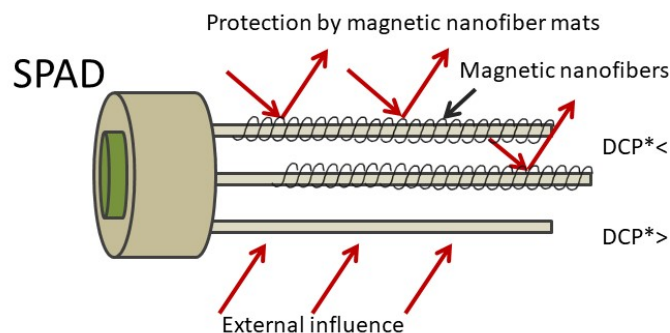


Figure 2. Schematic illustration of the novel single-photon avalanche diode (SPAD) design and the potential use of magnetic nanofiber mats to reduce external influences. The abbreviation (DCP*) means dark current pulses.

This study deals with electrospun magnetic nanofiber mats of polyacrylonitrile (PAN) and magnetite nanoparticles (Fe_3O_4) using the low toxic solvent dimethyl sulfoxide (DMSO). The different nanofiber morphologies of the nanofiber mats that were oxidatively stabilized and carbonized at 500 °C, 600 °C, 800 °C, and 1000 °C were investigated using Confocal laser Scanning Microscope (CLSM), Atomic Force Microscope (AFM), and Scanning Electron Microscope/Energy Dispersive X-Ray Spectroscopy (SEM/EDS), Fourier-transform infrared spectroscopy (FTIR) and are discussed below. The focus of this study is the carbonization of PAN/magnetite nanofiber mats at higher temperatures of up to 1000 °C and the characterization of the surface morphology of the resulting nanofiber mats. The novelty of this study is that, according to our research and to the best of our knowledge, there is no comparable study describing exactly this composition of PAN/magnetic nanofibers, such as 14% PAN and 20% magnetite, using low-toxic solvent DMSO, produced by needle-free electrospinning machine Nanospider[®] Lab and carbonization at 1000 °C, and focusing on morphology of these nanofiber mats.

The properties of such magnetic carbon nanofiber mats are promising for a novel construction design of SPAD where these properties are advantageous. The high conductivity, the excellent mechanical properties as well as the large magnetization and shielding against electromagnetic interference of magnetic carbon nanofibers can reduce noise in (SPAD) sensors and increase the speed of transmission of signals, and the present work aims to provide the basis for this application.

2. Materials and Methods

The polymer spinning solution contains 14 wt.% polyacrylonitrile (X-PAN, Dralon, Dormagen, Germany) dissolved in low-toxic solvent dimethyl sulfoxide (DMSO) (min. 99.9%, purchased from S3 chemicals, Bad Oeynhausen, Germany) and 20% magnetic nanoparticles Fe_3O_4 (magnetite, 50–100 nm diameter, Merck KGaA, Darmstadt, Germany). The polymer solution was stirred in a magnetic stirrer for 2 h and before electrospinning additionally treated in an ultrasonic bath for 40 min at 35 °C with a frequency of 37 kHz. The needleless electrospinning machine Nanospider Lab (Elmarco, Liberec, Czech Republic) was applied.

The nanofibers were produced at the following spinning parameters: High voltage 80 kV, electrode-substrate distance 240 mm, bottom-substrate distance 50 mm, nozzle diameter 0.9 mm, carriage speed 150 mm/s. The temperature in the chamber was 22 °C and relative humidity was 33%. The duration of electrospinning amounted to 15 min.

In our previous studies, it was experimentally found that the polymer amount between 14% and 16% of PAN dissolved in DMSO and the electrospinning parameters used in this study are most suitable for the production of homogeneous nanofibers using the electrospinning machine Nanospider[®] Lab [1,2,4,21,27,58,81].

Oxidative stabilization of the nanofiber mats was carried out in an oven (Nabertherm, Lilienthal, Germany). The typical stabilization temperature at 280 °C with a heating rate of 1 K/min was applied. Afterwards, an isothermal treatment was carried out at this final temperature for 1 h. Carbonization occurred in a furnace (Carbolite Gero, Neuhausen, Germany). The carbonization temperatures were set to 500 °C, 600 °C, 800 °C, and 1000 °C at a heating rate of 10 K/min in a nitrogen flow of 150 mL/min (STP). After reaching the final temperature, isothermal treatment was performed for 1 h.

Nanofiber diameters were examined based on analysis of SEM micrographs using ImageJ (software version 1.53e, 2021, National Institutes of Health, Bethesda, MD, USA). For the determination of the nanofiber diameter distribution, 100 fibers were measured.

Optical investigations were made with a FlexAFM Axiom (Nanosurf, Liestal, Switzerland) and a confocal laser scanning microscope (CLSM), VK-8710 (Keyence). A Zeiss 1450VPSE scanning electron microscope (SEM) and energy-dispersive X-ray spectroscopy (EDS) were used for more detailed investigations. For Fourier-transform infrared (FTIR) spectroscopy, an Excalibur 3100 (Varian, Inc., Palo Alto, CA, USA) was used. The spectral range from 4000 cm⁻¹ to 700 cm⁻¹ was set and 32 scans were averaged in each case and atmospheric noise was corrected.

3. Results

The morphologies of the studied nanofiber mats are shown in the CLSM micrographs in Figure 3. The color change with the increase in temperature and the brown color is clearly recognizable (see Figure 3b–d). According to our visual observations from previous studies [58,82–84] the color of nanofiber mats changes from white to brown during thermal treatment and to dark brown at 800 °C.

In CLSM micrographs, the color change looks different, from light gray (Figure 3a) to brown (Figure 3b) after stabilization, and carbonized nanofiber mats (Figure 3c) look gray with the light brown again (see Figure 3e,f). Interestingly, the color brown remains visible during carbonization at 600 °C, which is atypical compared to previous studies [15,83]. The reason for this is probably that the Fe₃O₄ particles in the sample carbonized at 600 °C are visible, which is not the case when pure PAN is carbonized and normally represents light gray color of the surfaces of the nanofiber mat in CLSM image [15,83]. This assumption is confirmed in further CLSM images, because even at higher carbonization temperatures like 800 °C and 1000 °C, the Fe₃O₄ particles are still faintly visible as light brown dots. The other reason for this finding could be that, presumably, only a small part of the sample used for the CLSM studies is presented here, which is not representative of the whole sample and therefore led to these unexpected results.

For more in-depth investigations of the surface morphology and characterization of the nanofibers, PAN/magnetite mats were investigated by AFM and SEM to complement CLSM observations.

Figure 4 shows AFM micrographs of magnetite nanofibers after electrospinning (Figure 4a), stabilization (Figure 4b), and carbonization at 600 °C (Figure 4c). After electrospinning, the nanofibers are relatively straight, linked together and some beads are visible. After oxidative stabilization at 280 °C (Figure 4b) and carbonization at 600 °C (Figure 4c), the nanofibers exhibit contraction. Moreover, from a visual point of view, the diameter of the nanofibers seems to decrease when increasing the temperature up to 600 °C.

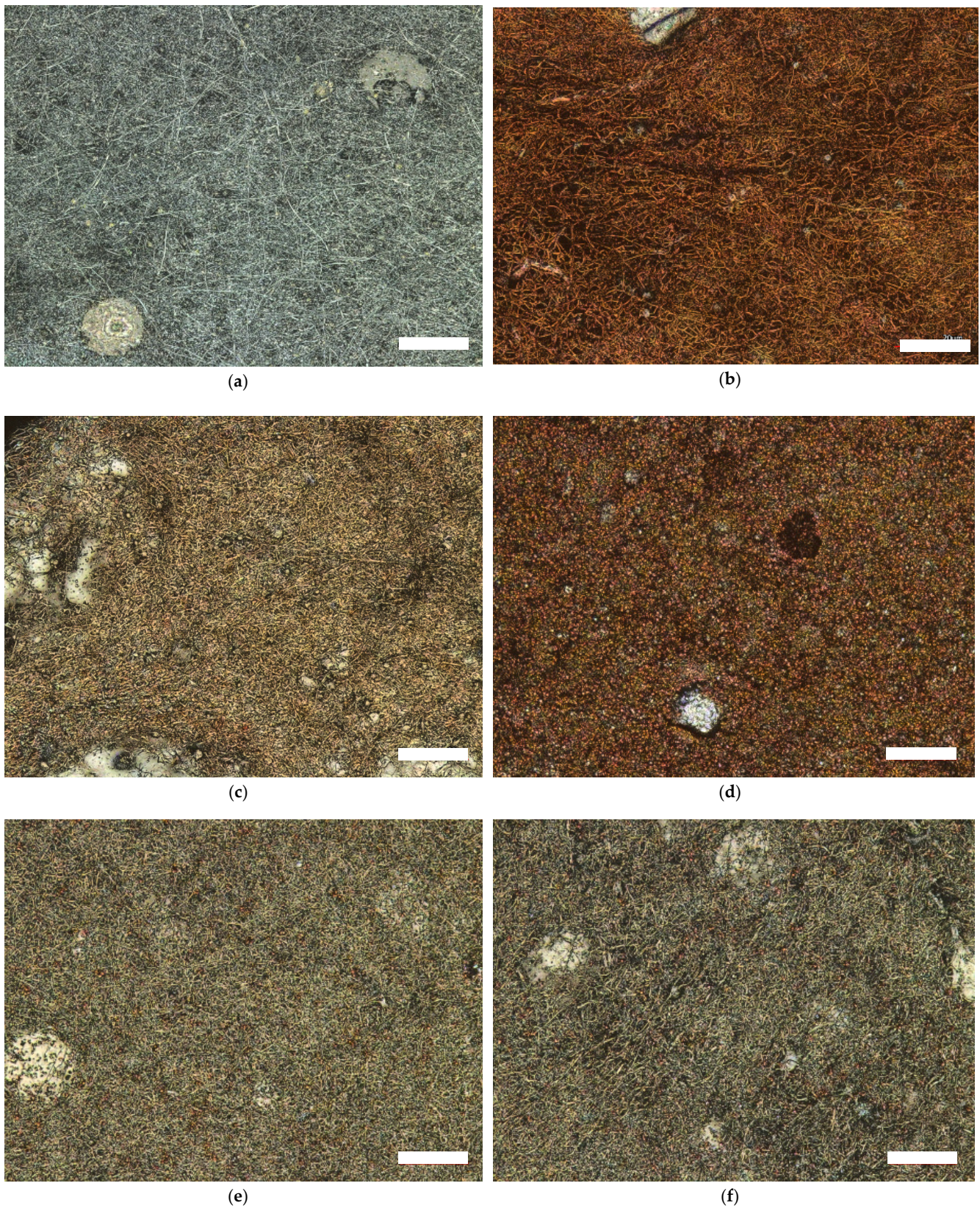


Figure 3. Confocal laser Scanning Microscope (CLSM) micrographs of PAN/magnetite nanofiber mats after electrospinning (a), after stabilization at 280 °C (b), after thermal treatment at 500 °C (c), at 600 °C (d), at 800 °C (e), and at 1000 °C (f). The scale bars indicate 20 μm.

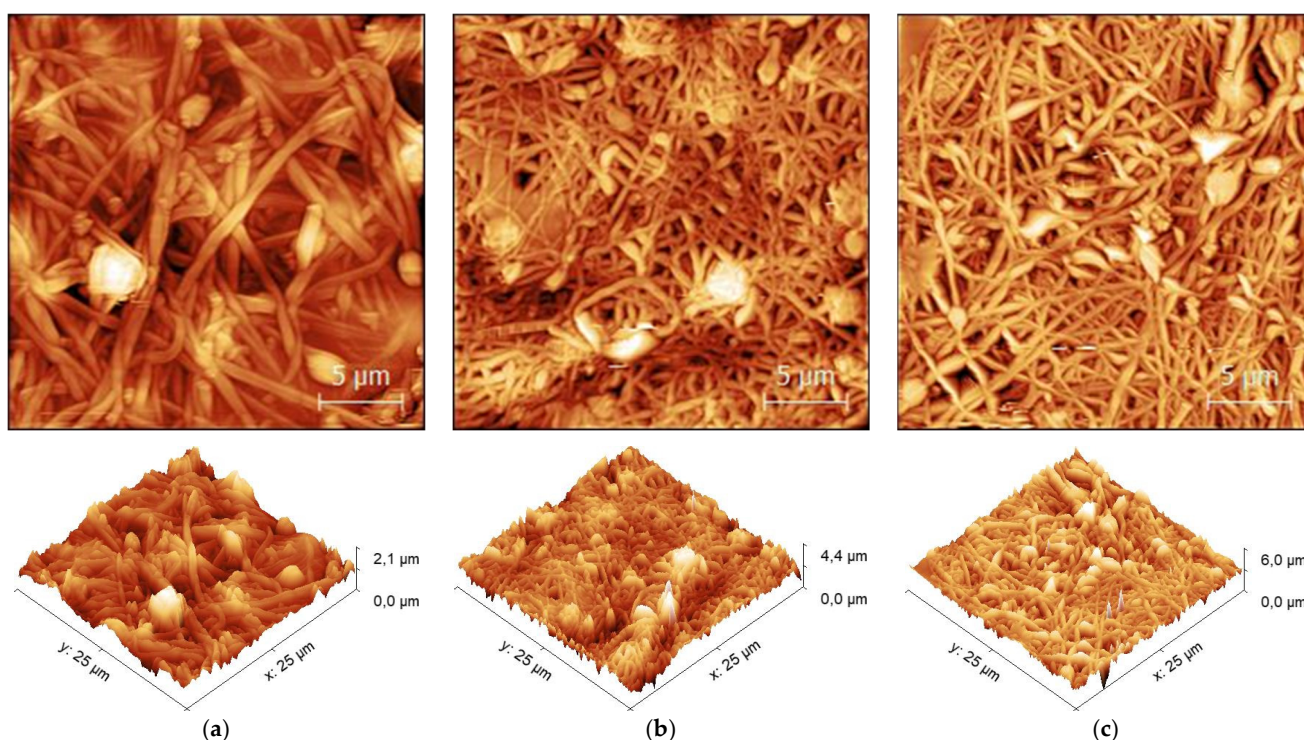


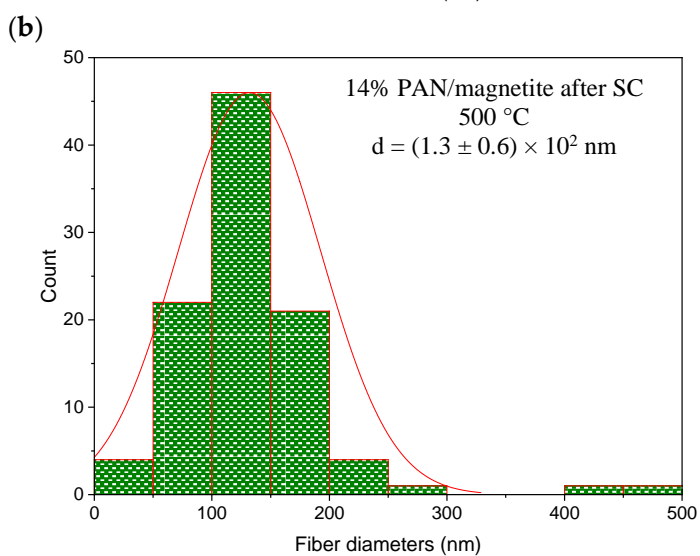
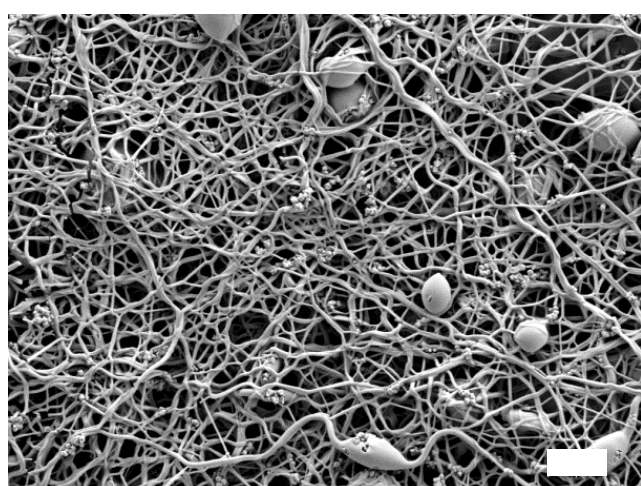
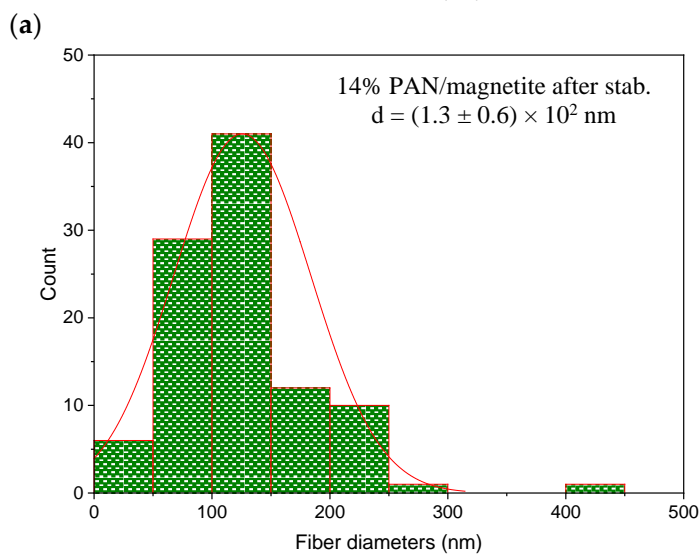
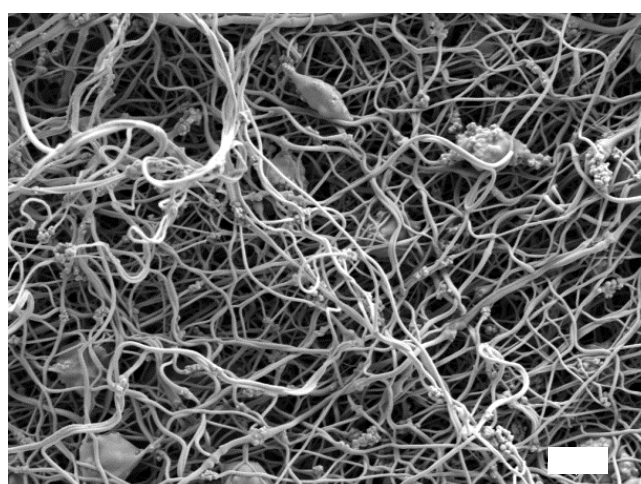
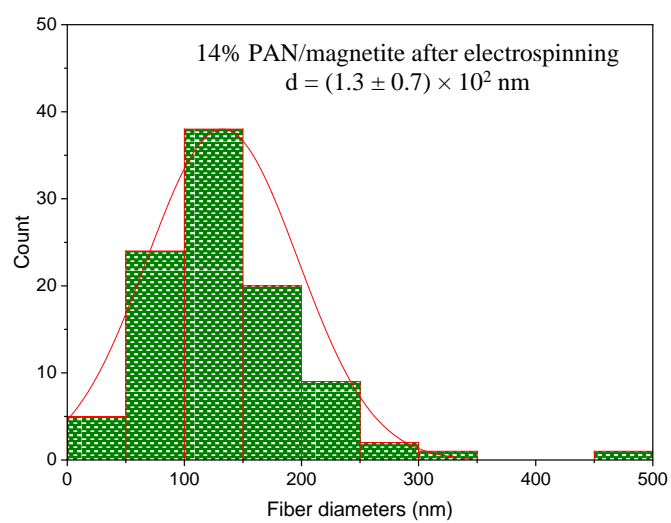
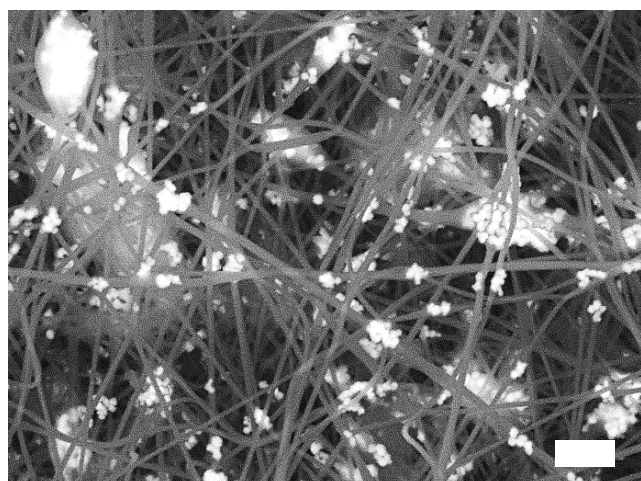
Figure 4. Atomic Force Microscope (AFM) micrographs of (a) PAN/magnetite nanofiber mat after electrospinning, (b) stabilized at 280 °C, and (c) carbonized at 600 °C. The scale bars indicate 5 μm.

The SEM micrographs and the graphs with nanofiber diameter in Figure 5 cannot confirm all the findings that were derived from the AFM micrographs (see Figure 5). The reason for this could be that the microscopic micrographs show only a small area of the sample and therefore do not represent the entire sample, as stated in the study by Wortmann et al. [85].

After the stabilization process, the fiber diameter decreases from $(1.3 \pm 0.7) \times 10^2$ nm to $(1.3 \pm 0.6) \times 10^2$, as was also suspected due to the AFM image (see Figure 4b) and corresponds to the SEM image (see Figure 5b) of the stabilized nanofiber mat.

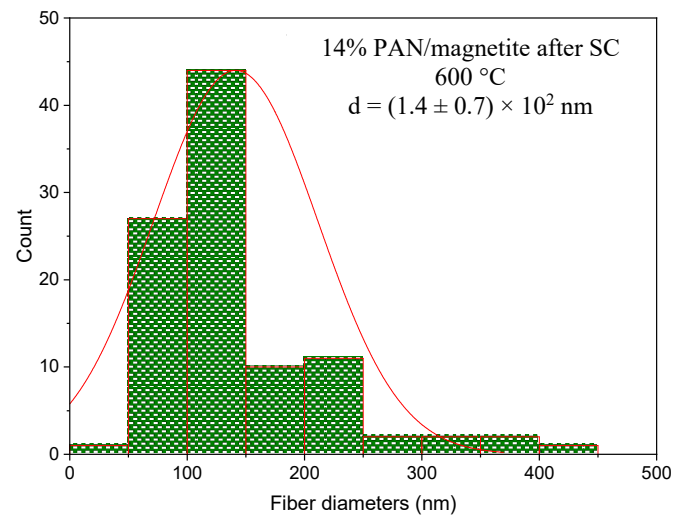
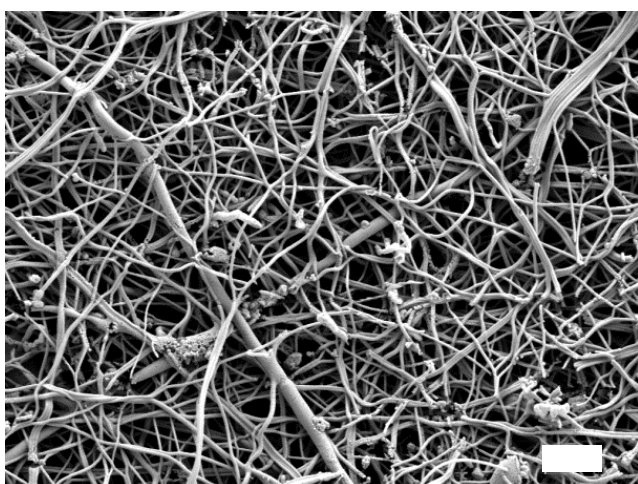
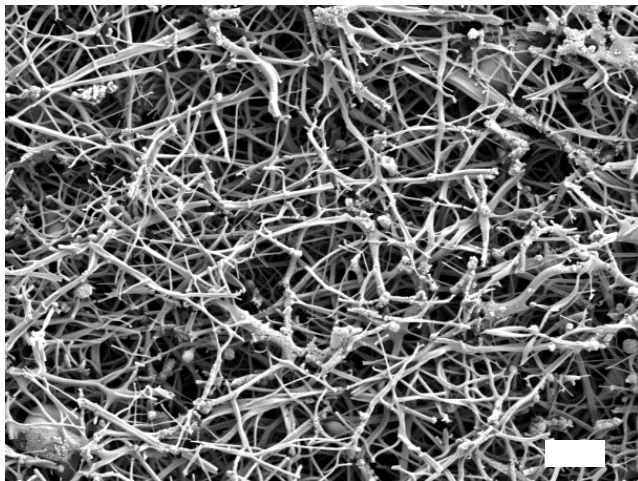
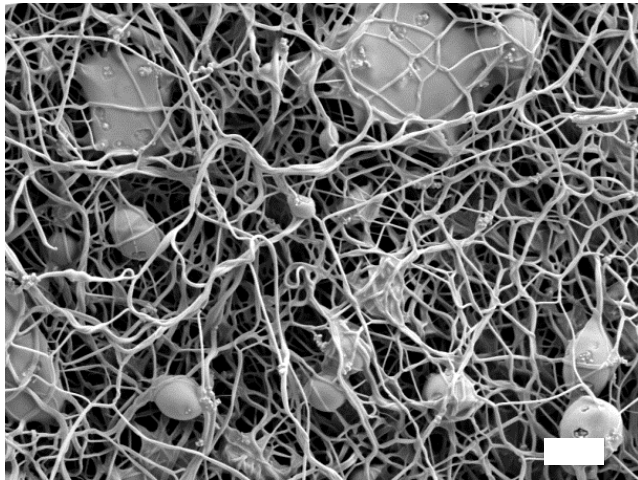
According to Figure 5c, which shows incipient carbonization at 500 °C, fiber diameter increases almost up to the previous thermally untreated state, which was after electrospinning and exhibits $(1.3 \pm 0.6) \times 10^2$ nm. With further increasing the carbonization temperature from 600 °C up to 1000 °C, the nanofiber diameter increased from $(1.4 \pm 0.7) \times 10^2$ nm at 600 °C to $(1.7 \pm 0.9) \times 10^2$ at 800 °C and finally reached $(1.8 \pm 0.8) \times 10^2$ nm at 1000 °C (see Figure 5e,f).

By observing the surface morphology of the nanofiber mats, it was found that the nanofibers after electrospinning have relatively straight nanofibers with some beads and aggregations of magnetic particles in both AFM image (Figure 4a) and SEM image (Figure 5a). After stabilization at 280 °C, the nanofibers contract noticeably, form networks, and no longer behave as single fibers (See Figure 4b,c). With further increase of carbonization temperature from 500 °C to 600 °C, the morphology of nanofibers does not seem to change significantly and hardly any difference is seen (see Figures 4c and 5c,d). It should be noted that the nanofibers continue to be more contracted in comparison to stabilized nanofiber mats (see Figures 4c and 5c,d). The nanofiber mats carbonized at 800 °C (Figure 5e) and 1000 °C (Figure 5f) differ from the carbonization at the lower temperatures of 500 °C (Figure 5c) and 600 °C (Figure 5d) in that they are more contracted but show straighter fibers and exhibit some fractures, and the aggregation of nanoparticles is more visible than at the previous carbonization temperatures.

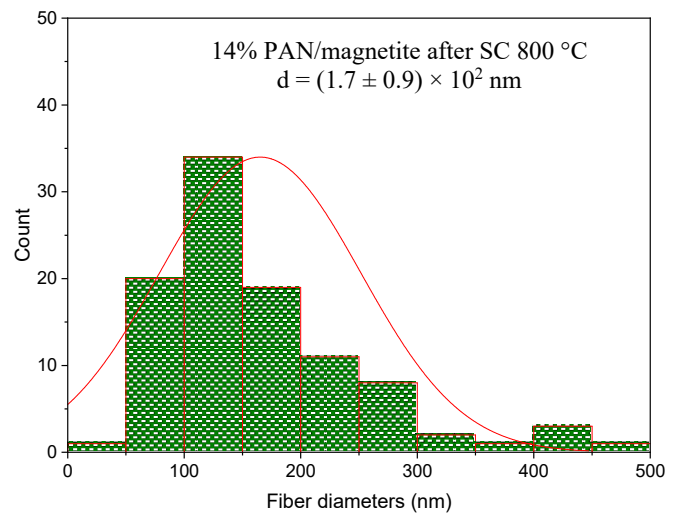


(c)

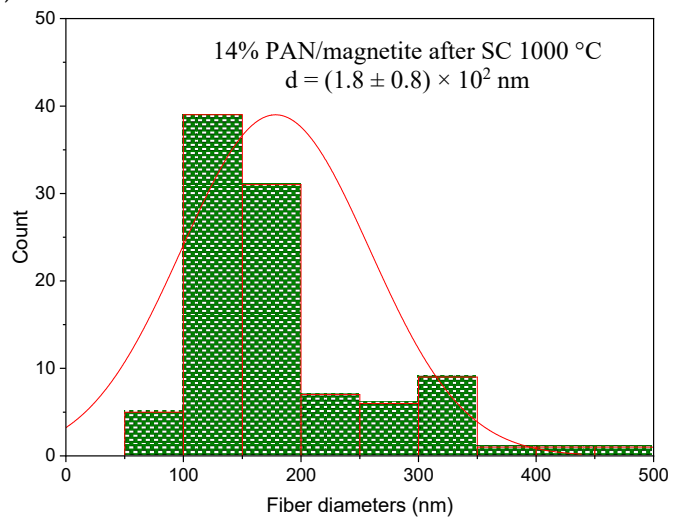
Figure 5. Cont.



(d)



(e)



(f)

Figure 5. Scanning Electron Microscope (SEM) micrographs and distributions of the fiber diameters of (a) PAN/magnetite nanofiber mat after electrospinning, (b) stabilized at 280 °C, (c) carbonized at 500 °C, (d) carbonized at 600 °C, (e) carbonized at 800 °C, and (f) carbonized at 1000 °C. The scale bars indicate 2 μ m.

Interestingly, similarly to the study by Fokin et al. [58], the beads in the nanofiber mats almost completely disappeared at 800 °C (see Figure 5d). Furthermore, the beads are no longer visible at higher carbonization temperatures of 1000 °C (see Figure 5e). In order to preserve the beads at higher carbonization temperatures, strategies should be developed in the near future.

As known from previous studies, by adding particles or other polymers into PAN polymer, the diameter of nanofibers increases compared to pure PAN nanofibers [58,82]. Furthermore, the dimensional stability under thermal treatment is improved and the nanofiber mats contract less, are more flexible and not as fragile compared to pure PAN nanofiber mats [58,69,86].

In the study of Trabelsi et al., the PAN/magnetite nanofiber diameter after electrospinning amounted to $(1.8 \pm 0.5) \times 10^2$ nm [21], in the study of Döpke et al. [2] to $(1.2 \pm 0.4) \times 10^2$ nm and in the study of Fokin et al. to $(1.0 \pm 0.5) \times 10^2$ nm [58]. The diameter of nanofibers in this study amounts to $(1.3 \pm 0.7) \times 10^2$ nm and a significant difference between the results and other studies [2,21,58] was not observed. In general, it could be stated that the nanofiber diameter of PAN/magnetite nanofiber mats after electrospinning [2,21,58], as well as stabilization and carbonization at 500 °C and 800 °C [58], is not significantly different from previous studies. In the study by Fokin et al., the PAN/magnetite nanofiber diameter after stabilization amounted to $(1.7 \pm 0.7) \times 10^2$ nm [58] and in this study to $(0.1 \pm 0.6) \times 10^2$ nm and after carbonization at 500 °C amounted to $(1.4 \pm 0.5) \times 10^2$ nm and in this study to $(1.3 \pm 0.6) \times 10^2$ nm. Moreover, the nanofiber diameter after carbonization at 800 °C was $(2.0 \pm 0.9) \times 10^2$ nm in the case of Fokin et al. [58] and $(1.8 \pm 0.8) \times 10^2$ nm in this study. However, it should also be mentioned that these differences in nanofiber diameter are not significant statistically due to the wide dispersion of the measured fiber diameters. In addition, the arbitrary choice of the investigated sample areas also partly plays a role.

FTIR measurements were performed on the PAN/magnetite nanofiber mats after electrospinning, stabilization, and carbonization at 500 °C, 600 °C, 800 °C, and 1000 °C (see Figure 6).

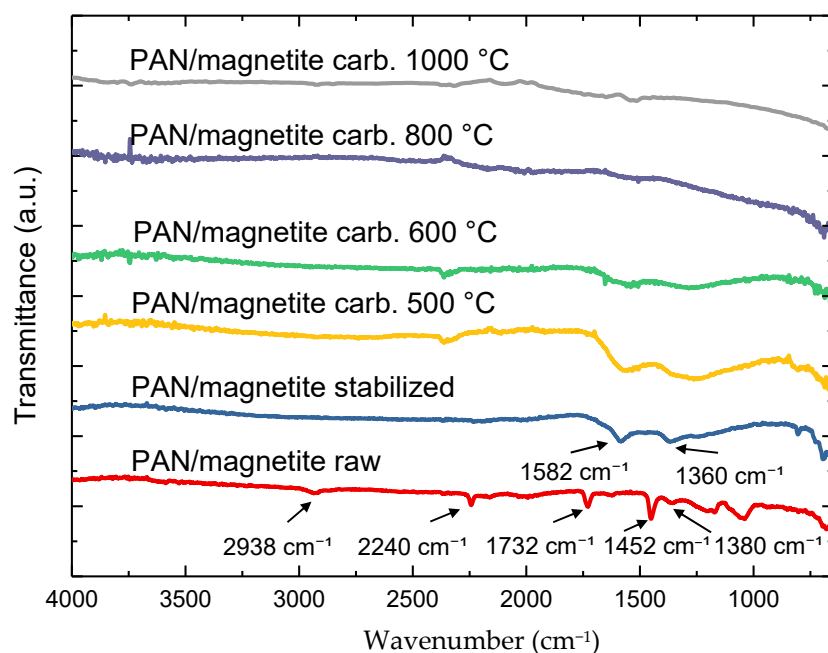


Figure 6. Fourier-transform infrared spectroscopy (FTIR) measurements of PAN/magnetite samples after electrospinning, stabilization, and carbonization at 500 °C, 600 °C, 800 °C, and 1000 °C. The lines are vertically offset for clarity.

The comparison of the spectra shows that the transmittance of PAN/magnetite mats consists of the typical PAN peaks. Significant changes occur during the stabilization and carbonization processes and almost all the peaks disappear at carbonization at 800 °C or higher. Below 800 °C, according to our previous study [58], carbonization is not complete, and the peaks are visible.

The stretching vibrations of the C≡N nitrile functional group at 2240 cm⁻¹ and the carbonyl (C=O) stretching peak at 1732 cm⁻¹ can be observed. In addition, the bending and stretching vibrations of CH₂ at 2938 cm⁻¹, 1452 cm⁻¹, and 1380 cm⁻¹ can be identified. This characterization of the nanofiber mats is well-known from previous studies [84–86].

In FTIR spectra of the stabilized nanofiber mats, the most prominent peaks are those of C=N stretching vibrations at 1582 cm⁻¹, C=C stretching vibration at 1660 cm⁻¹, as well as C-H bending and C-H₂ wagging around 1360 cm⁻¹ [58].

As found in a previous study, the temperature treatment at 500 °C is not sufficient to achieve complete carbonization and leads to incipient carbonization [87]. This is confirmed in the FTIR spectrum, which still looks very similar to the stabilized sample (see Figure 6). After carbonization at 600 °C, the peaks disappeared almost completely and when carbonized at 800 °C and 1000 °C, only a few functional groups remained, resulting in the typical high absorption of carbon. As can be seen in the FTIR, the complete carbonization occurs at 800 °C, as known from our previous studies [82,83,86]. Moreover, similarly to our previous study [58], when comparing the FTIR measurements with those on pure PAN nanofiber mats or PAN mixtures with TiO₂, gelatin, etc., no significant difference could be detected due to the embedded magnetic nanoparticles [58,82,86].

Carbonization at high temperatures above 800 °C is challenging because as the temperature increases, the nanofiber morphology also changes due to the incited chemical processes. At this point, defined surface morphology should be weighed up against the applied carbonization temperature. From previous studies it is known that the nanofiber mats are relatively flexible after electrospinning; after stabilization and carbonization, however, they lose flexibility either partially or completely and become very fragile at carbonization higher than 800 °C [15,58,82,83]. Therefore, the carbonization temperature of 1000 °C was relatively challenging for PAN/magnetite mats and confirmed the assumption that the desired surface morphology and carbonization temperature should be considered to obtain desirable magnetic carbon nanofibers for defined applications. As can be seen in FTIR, after carbonization at 1000 °C, almost all the functional groups have disappeared and become the similar structure of graphite fibers [88].

It is known from literature that the conductivity increases with increasing carbonization temperature [89,90]. The study by Liu et al. confirms the increase in the conductivity of carbon nanofibers prepared from PAN precursor with increasing temperature. At 400 °C, the conductivity of the carbon fibers has reached 0.015 S·cm⁻¹ and at 700 °C, 0.018 S·cm⁻¹. Moreover, the conductivity increases significantly with carbonization at 1000 °C and attains 105.44 S·cm⁻¹ [90].

There are various reasons for the increase in conductivity. On the one hand, the fiber diameter decreases due to the prevailing chemical processes in the heat treatment process. On the other hand, the preferred orientation of the carbon layer with a flat structure increases significantly, while the void volume fraction and the crystallite size increase significantly [90]. During the carbonization process, various processes such as oxidation, aromatization, cyclization, dehydrogenation, and crosslinking occurred [91–93]. The increase in temperature leads to the coalescence of the flake structures, which are oriented along the longitudinal direction, and this finally leads to a significant increase in conductivity [90,92]. For this reason, carbon nanofibers carbonized at 1000 °C showed a sufficient degree of carbonization and structural integrity [90].

To investigate the distribution of magnetite in the samples in more detail, SEM image and EDS mapping were used. When comparing the SEM image (Figure 7a) and the EDS map (Figure 7b), it is suggested that the highest particle concentration is located in the beads.

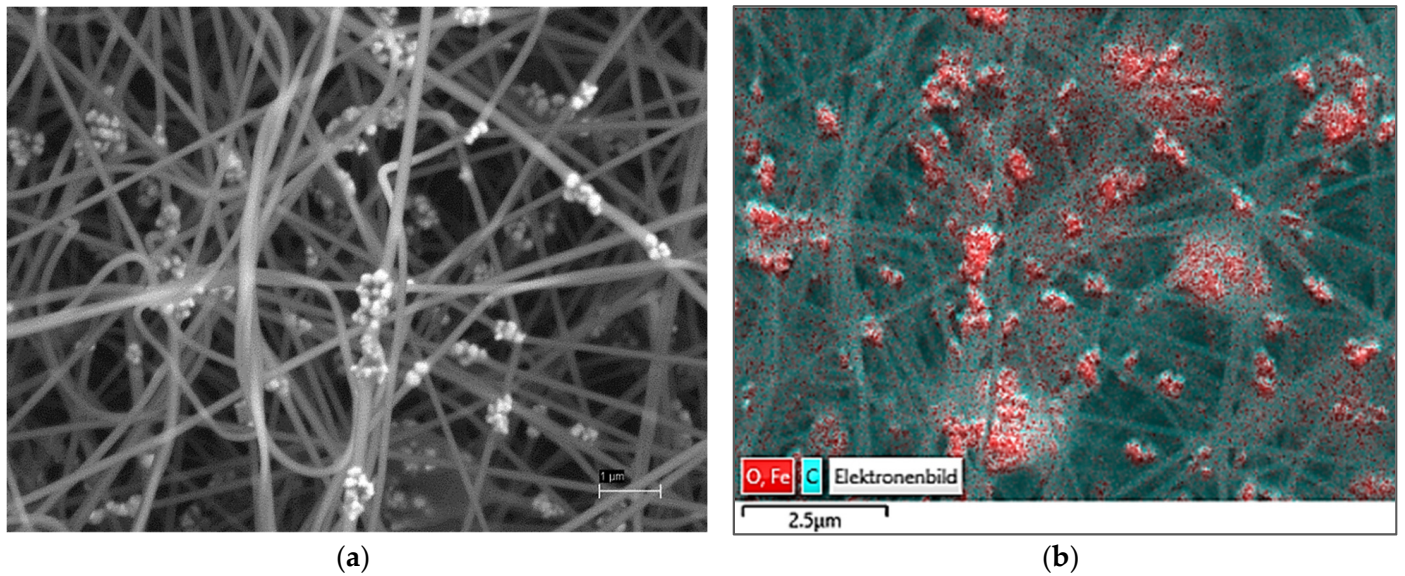


Figure 7. Scanning Electron Microscope (SEM) image of PAN/magnetite nanofiber mat (a) and Energy Dispersive X-Ray Spectroscopy (EDS) spectrum showing magnetite in red color (b). The scale bars indicate 1 μm (a) and 2.5 μm (b).

Figure 8 shows the surface scanned with EDS for a more detailed examination and the spectra of the materials inside this surface. As can be seen in the SEM image and marked with red frames, the EDS spectrum was recorded in a microscopic area of the sample (see Figure 8).

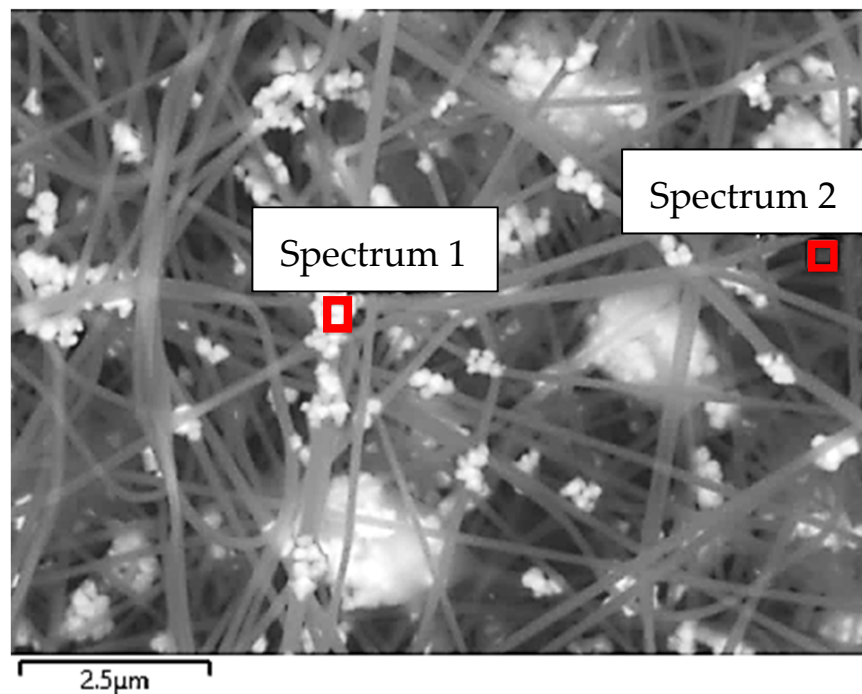
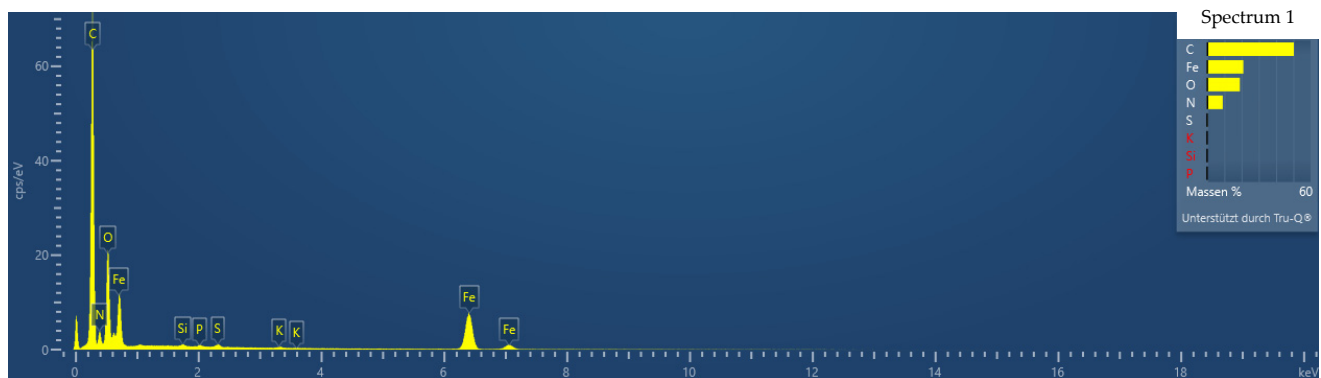


Figure 8. SEM image of PAN/magnetite nanofiber mat (a) spot on a bead (Spectrum 1); and (b) spot on a nanofiber (Spectrum 2). The scale bar indicate 2.5 μm .

The examined areas were marked with a red frame (see Figure 8) and the EDS spectra were generated for these areas (see Figure 9a,b). The first EDS (Spectrum 1) defines a small area where a bead is located, and the second EDS (Spectrum 2) was directed to nanofiber.



(a)



(b)

Figure 9. EDS spectra of PAN/magnetite nanofiber mat (a) spot on a bead; and (b) spot on a nanofiber.

It could be observed that carbon (C) is present in both EDS spectra in a large amount at 0.3 keV. The peaks at 0.7 keV, 6.4 keV, and 7.1 keV in both EDS spectra (see Figure 9a,b) can be identified as being related to iron (Fe). Looking at the EDS spectra 1 (Figure 9a), it is noticeable that the iron peak (Fe) is higher in the EDS spectrum 1 directed at the bead compared to the EDS spectrum 2 directed at the nanofiber. In addition, the EDS spectrum 1 shows strong peaks of the element iron (Fe), confirming that the magnetite nanoparticles are agglomerated within the beads. Similar to our previous study [21], larger amounts of magnetite can be suspected in beads than are expected to be present in nanofibers.

4. Conclusions

In this study, PAN/magnetite nanofiber mats were prepared by adding nanoparticles into a polymer solution used for needleless electrospinning method. Oxidative stabilization and carbonization at 500 °C, 600 °C, 800 °C, and 1000 °C were performed, and the resulting surface morphologies of the nanofiber mats were studied and discussed. According to this study, the addition of nanoparticles increased the fiber average and improved the dimensional stability. The agglomerations of magnetite nanoparticles were largely detected in beads by means of SEM and EDS spectra. Similar to our previous study [17], larger amounts of magnetite are suspected in the beads than in the nanofibers. The addition of nanoparticles changes the morphology of nanofiber mats. New types of nanofiber mats can be manufactured from numerous polymers and different raw materials, which can lead to defined functions and different sensor capacities and still allow for much innovation in the field of sensor technology.

Carbonization of nanofiber mats at 1000 °C is challenging because, due to the incited chemical processes, the surface morphology changes. The conductivity at high temperatures increases, which is beneficial for the speed of signal transmission when such magnetic carbon nanofiber mats will be used for the construction of novel single photon avalanche

diodes (SPADs), where these properties are advantageous. The excellent mechanical properties as well as the large magnetization and shielding against electromagnetic interference can reduce the noise in the (SPAD) sensor and increase the speed of signal transmission. This present work aims to provide the basis for this novel single photon avalanche diode (SPAD) construction design.

Author Contributions: Conceptualization, M.T., A.M. and L.S.; methodology, M.T., A.M., M.K., I.M., A.P., K.E. and L.S.; investigation, M.T., A.M., M.K. and L.S.; writing—original draft preparation, M.T., A.M., I.M., A.P. and L.S.; writing—review and editing, all authors; visualization, M.T., A.M., K.E. and L.S.; supervision, A.P., K.E. and L.S. All authors have read and agreed to the published version of the manuscript.

Funding: We acknowledge support by the Open Access Publication Fund of the Bielefeld University of Applied Sciences.

Institutional Review Board Statement: Not applicable.

Informed Consent Statement: Not applicable.

Data Availability Statement: The data created in this study are fully depicted in the article.

Acknowledgments: The authors acknowledge personal funding from the internal PhD funds of Bielefeld University of Applied Sciences, Erasmus+ and the internal funds for female students in STEM programs at Bielefeld University of Applied Sciences.

Conflicts of Interest: The authors declare no conflict of interest.

References

1. Storck, J.L.; Grothe, T.; Mamun, A.; Sabantina, L.; Klöcker, M.; Blachowicz, T.; Ehrmann, A. Orientation of Electrospun Magnetic Nanofibers Near Conductive Areas. *Materials* **2020**, *13*, 47. [CrossRef] [PubMed]
2. Döpke, C.; Grothe, T.; Steblinski, P.; Klöcker, M.; Sabantina, L.; Kosmalka, D.; Blachowicz, T.; Ehrmann, A. Magnetic Nanofiber Mats for Data Storage and Transfer. *Nanomaterials* **2019**, *9*, 92. [CrossRef]
3. Blachowicz, T.; Ehrmann, A. New Materials and Effects in Molecular Nanomagnets. *Appl. Sci.* **2021**, *11*, 7510. [CrossRef]
4. Trabelsi, M.; Mamun, A.; Klöcker, M.; Sabantina, L.; Großerhede, C.; Blachowicz, T.; Ehrmann, A. Increased Mechanical Properties of Carbon Nanofiber Mats for Possible Medical Applications. *Fibers* **2019**, *7*, 98. [CrossRef]
5. Yu, G.F.; Li, G.T.; Pan, W.; He, X.X.; Zhang, Y.J.; Gong, M.G.; Yu, M.; Zhang, Z.M.; Long, Y.Z. Electromagnetic functionalized ultrafine polymer/ γ -Fe₂O₃ fibers prepared by magnetic-mechanical spinning and their application as strain sensors with ultrahigh stretchability. *Compos. Sci. Technol.* **2017**, *139*, 1–7. [CrossRef]
6. Xue, J.; Wu, T.; Dai, Y.; Xia, Y. Electrospinning and electrospun nanofibers: Methods, materials, and applications. *Chem. Rev.* **2019**, *119*, 5298–5415. [CrossRef]
7. Liu, Q.; Zhu, J.; Zhang, L.; Qiu, Y. Recent advances in energy materials by electrospinning. *Renew. Sustain. Energy Rev.* **2018**, *81*, 1825–1858. [CrossRef]
8. Chen, S.X.; Li, R.Q.; Li, X.R.; Xie, J.W. Electrospinning: An enabling nanotechnology platform for drug delivery and re-generative medicine. *Adv. Drug Deliv. Rev.* **2018**, *132*, 188–213. [CrossRef]
9. Bhardwaj, N.; Kundu, S.C. Electrospinning: A fascinating fiber fabrication technique. *Biotechnol. Adv.* **2010**, *28*, 325–347. [CrossRef]
10. Yalcinkaya, F. A review on advanced nanofiber technology for membrane distillation. *J. Eng. Fibers Fabr.* **2019**, *14*, 1558925018824901. [CrossRef]
11. Sasithorn, N.; Martinová, L.; Horáková, J.; Mongkholrattanasit, R. Fabrication of Silk Fibroin Nanofibres by Needleless Electrospinning, Electrospinning—Material, Techniques, and Biomedical Applications, Sajjad Haider and Adnan Haider. *IntechOpen* **2016**, 95–113. Available online: <https://www.intechopen.com/chapters/52866> (accessed on 18 November 2021). [CrossRef]
12. Grothe, T.; Storck, J.L.; Dotter, M.; Ehrmann, A. Impact of solid content in the electrospinning solution on physical and chemical properties of polyacrylonitrile (PAN) nanofibrous mats. *Tekstilec* **2020**, *63*, 225–232. [CrossRef]
13. Tanzli, E.; Ehrmann, A. Electrospun Nanofibrous Membranes for Tissue Engineering and Cell Growth. *Appl. Sci.* **2021**, *11*, 6929. [CrossRef]
14. Ehrmann, A. Non-Toxic Crosslinking of Electrospun Gelatin Nanofibers for Tissue Engineering and Biomedicine—A Review. *Polymers* **2021**, *13*, 1973. [CrossRef]
15. Storck, J.L.; Hellert, C.; Brockhagen, B.; Wortmann, M.; Diestelhorst, E.; Frese, N.; Grothe, T.; Ehrmann, A. Metallic Supports Accelerate Carbonization and Improve Morphological Stability of Polyacrylonitrile Nanofibers during Heat Treatment. *Materials* **2021**, *14*, 4686. [CrossRef]

16. Hellert, C.; Storck, J.L.; Grothe, T.; Kaltschmidt, B.; Hütten, A.; Ehrmann, A. Positioning and aligning electrospun PAN fibers by conductive and dielectric substrate patterns. *Macromol. Symp.* **2021**, *395*, 2000213. [[CrossRef](#)]
17. Díaz Silva, N.; Valdez Salas, B.; Nedev, N.; Curiel Alvarez, M.; Bastidas Rull, J.M.; Zlatev, R.; Stoytcheva, M. Synthesis of Carbon Nanofibers with Maghemite via a Modified Sol-Gel Technique. *J. Nanomater.* **2017**, *2017*, 5794312. [[CrossRef](#)]
18. Lavagna, L.; Nisticò, R.; Musso, S.; Pavese, M. Functionalization as a way to enhance dispersion of carbon nanotubes in matrices: A review. *Mater. Today Chem.* **2021**, *20*, 100477. [[CrossRef](#)]
19. Lake, C.L.; Lake, P.D. Chapter 11—Carbon Nanofiber Multifunctional Mat. In *Nanotube Superfiber Materials*; Schulz, M.J., Shanov, V.N., Yin, Z., Eds.; William Andrew Publishing: Norwich, NY, USA, 2014; pp. 313–331. [[CrossRef](#)]
20. Kang, I.; Heung, Y.Y.; Kim, J.H.; Lee, J.W.; Gollapudi, R.; Subramaniam, S.; Narasimhadevara, S.; Hurd, D.; Kirikera, G.R.; Shanov, V.; et al. Introduction to carbon nanotube and nanofiber smart materials. *Compos. Part B Eng.* **2006**, *37*, 382–394. [[CrossRef](#)]
21. Trabelsi, M.; Mamun, A.; Klöcker, M.; Sabantina, L. Investigation of metallic nanoparticle distribution in PAN/magnetic nanocomposites fabricated with needleless electrospinning technique. *Commun. Dev. Assem. Text. Prod.* **2021**, *2*, 8–17. [[CrossRef](#)]
22. Blachowicz, T.; Grzybowski, J.; Steblinski, P.; Ehrmann, A. Neuro-Inspired Signal Processing in Ferromagnetic Nanofibers. *Biomimetics* **2021**, *6*, 32. [[CrossRef](#)]
23. Amini, F.; Blachowicz, T.; Ehrmann, A. Systematic study of magnetization reversal in beaded fibers from different magnetic materials. *J. Magn. Magn. Mater.* **2021**, *529*, 167855. [[CrossRef](#)]
24. Pljonkin, A.; Singh, P.K.; Joshi, S.; Sabantina, L. The Study of Synchronization in Quantum Key Distribution System. In *Futuristic Trends in Network and Communication Technologies*; FTNCT 2020, Communications in Computer and Information Science; Singh, P.K., Veselov, G., Pljonkin, A., Kumar, Y., Paprzycki, M., Zachinyaev, Y., Eds.; Springer: Singapore, 2021; Volume 1396, pp. 68–80. [[CrossRef](#)]
25. Pljonkin, A.; Petrov, D.; Sabantina, L.; Dakhkilgova, K. Nonclassical Attack on a Quantum Key Distribution System. *Entropy* **2021**, *23*, 509. [[CrossRef](#)]
26. Atif, R.; Inam, F. Reasons and remedies for the agglomeration of multilayered graphene and carbon nanotubes in polymers. *Beilstein J. Nanotechnol.* **2016**, *7*, 1174–1196. [[CrossRef](#)] [[PubMed](#)]
27. Sabantina, L.; Hes, L.; Rodríguez-Mirasol, J.; Cordero, T.; Ehrmann, A. Water vapor permeability through PAN nanofiber mat with varying membrane-like areas. *Fibres Text. East. Eur.* **2019**, *27*, 12–15. [[CrossRef](#)]
28. Sabantina, L.; Rodríguez-Mirasol, J.; Cordero, T.; Finsterbusch, K.; Ehrmann, A. Investigation of needleless electrospun PAN nanofiber mats. *AIP Conf. Proc.* **2018**, *1952*, 020085. [[CrossRef](#)]
29. Wehlage, D.; Böttjer, R.; Grothe, T.; Ehrmann, A. Electrospinning water-soluble/insoluble polymer blends. *AIMS Mater. Sci.* **2018**, *5*, 190–200. [[CrossRef](#)]
30. Grothe, T.; Brikmann, V.; Meissner, H.; Ehrmann, A. Influence of Solution and Spinning Parameters on Nanofiber Mat Creation of Poly(ethylene oxide) by Needleless Electrospinning. *Mater. Sci.* **2017**, *23*, 342–349. [[CrossRef](#)]
31. Mamun, A.; Blachowicz, T.; Sabantina, L. Electrospun Nanofiber Mats for Filtering Applications—Technology, Structure and Materials. *Polymers* **2021**, *13*, 1368. [[CrossRef](#)]
32. Blachowicz, T.; Ehrmann, G.; Ehrmann, A. Textile-Based Sensors for Biosignal Detection and Monitoring. *Sensors* **2021**, *21*, 6042. [[CrossRef](#)]
33. Ruiz-Rosas, R.; Bedia, J.; Rosas, J.M.; Lallave, M.; Loscertales, I.G.; Rodríguez-Mirasol, J.; Cordero, T. Methanol decomposition on electrospun zirconia nanofibers. *Catal. Today* **2012**, *187*, 77–87. [[CrossRef](#)]
34. García-Mateos, F.J.; Ruiz-Rosas, R.; Rosas, J.M.; Rodríguez-Mirasol, J.; Cordero, T. Controlling the Composition, Morphology, Porosity, and Surface Chemistry of Lignin-Based Electrospun Carbon Materials. *Front. Mater.* **2019**, *6*, 114. [[CrossRef](#)]
35. Moulefera, I.; Trabelsi, M.; Mamun, A.; Sabantina, L. Electrospun Carbon Nanofibers from Biomass and Biomass Blends—Current Trends. *Polymers* **2021**, *13*, 1071. [[CrossRef](#)] [[PubMed](#)]
36. Rothschild, A.; Komem, Y. The effect of grain size on the sensitivity of nanocrystalline metal-oxide gas sensors. *J. Appl. Phys.* **2004**, *95*, 6374–6380. [[CrossRef](#)]
37. Blachowicz, T.; Ehrmann, A. Shielding of Cosmic Radiation by Fibrous Materials. *Fibres* **2021**, *9*, 60. [[CrossRef](#)]
38. Panapoy, M.; Dankeaw, A.; Ksapabut, B. Electrical Conductivity of PAN-based Carbon Nanofibers Prepared by Electrospinning Method. *Thammasat Int. J. Sc. Tech* **2008**, *13*, 11–17.
39. Wang, Z.; Wu, S.; Wang, J.; Yu, A.; Wei, G. Carbon Nanofiber-Based Functional Nanomaterials for Sensor Applications. *Nanomaterials* **2019**, *9*, 1045. [[CrossRef](#)]
40. Wang, C.; Yin, L.; Zhang, L.; Xiang, D.; Gao, R. Metal oxide gas sensors: Sensitivity and influencing factors. *Sensors* **2010**, *10*, 2088–2106. [[CrossRef](#)]
41. Barsan, N.; Weimar, U. Conduction model of metal oxide gas sensors. *J. Electroceram.* **2001**, *7*, 143–167. [[CrossRef](#)]
42. Ali, M.A.; Mondal, K.; Singh, C.; Malhotra, B.D.; Sharma, A. Anti-epidermal growth factor receptor conjugated meso-porous zinc oxide nanofibers for breast cancer diagnostics. *Nanoscale* **2015**, *7*, 7234–7245. [[CrossRef](#)]
43. Chowdhury, A.D.; De, A.; Chaudhuri, C.R.; Bandyopadhyay, K.; Sen, P. Label free polyaniline based impedimetric bi-sensor for detection of E. coli O157: H7 Bacteria. *Sens. Actuators B Chem.* **2012**, *171–172*, 916–923. [[CrossRef](#)]
44. Zhang, Y.; Wang, Y.; Jia, J.; Wang, J. Nonenzymatic glucose sensor based on graphene oxide and electrospun NiO nanofibers. *Sens. Actuators B Chem.* **2012**, *171*, 580–587. [[CrossRef](#)]

45. Luo, Y.; Nartker, S.; Miller, H.; Hochhalter, D.; Wiederoder, M.; Wiederoder, S. Surface functionalization of electrospun nanofibers for detecting *E. coli* O157: H7 and BVDV cells in a direct-charge transfer biosensor. *Biosens. Bioelectron.* **2010**, *26*, 1612–1617. [[CrossRef](#)]
46. Bahrami, G.; Ehzari, H.; Mirzabeigy, S.; Mohammadi, B.; Arkan, E. Fabrication of a sensitive electrochemical sensor based on electrospun magnetic nanofibers for morphine analysis in biological samples. *Mater. Sci. Eng. C* **2020**, *106*, 110183. [[CrossRef](#)] [[PubMed](#)]
47. Guarino, V.; Iannotti, V.; Ausanio, G.; Ambrosio, L.; Lanotte, L. Elastomagnetic nanofiber wires by magnetic field assisted electrospinning. *Express Polym. Lett.* **2019**, *13*, 419–428. [[CrossRef](#)]
48. Li, J.; Chen, X.; Xu, D.; Pan, K. Immobilization of horseradish peroxidase on electrospun magnetic nanofibers for phenol removal. *Ecotoxicol. Environ. Saf.* **2019**, *170*, 716–721. [[CrossRef](#)] [[PubMed](#)]
49. Sung, Y.K.; Ahn, B.W.; Kang, T.J. Magnetic nanofibers with core (Fe₃O₄ nanoparticle suspension)/sheath (poly ethylene terephthalate) structure fabricated by coaxial electrospinning. *J. Magn. Magn. Mater.* **2012**, *324*, 916–922. [[CrossRef](#)]
50. Wang, B.; Sun, Y.H.W. Preparation and properties of electrospun PAN/Fe₃O₄ magnetic nanofibers. *J. Appl. Polym. Sci.* **2010**, *116*, 2658–2667. [[CrossRef](#)]
51. Wang, Y.; Santiago-Aviles, J.J. Low-Temperature Electronic Properties of Electrospun PAN Derived Carbon Nanofiber. *IEEE Trans. Nanotechnol.* **2004**, *3*, 221–224. [[CrossRef](#)]
52. Guadagno, L.; Raimondo, M.; Vittoria, V.; Vertuccio, L.; Lafdi, K.; De Vivo, B.; Lamberti, P.; Spinelli, G.; Tucci, V. The role of carbon nanofiber defects on the electrical and mechanical properties of CNF-based resins. *Nanotechnology* **2013**, *24*, 305704. [[CrossRef](#)]
53. Lu, W.; Wang, T.; He, X.; Sun, K.; Huang, Z.; Tan, G.; Eddings, E.G.; Adidharma, H.; Fan, M. A new method for preparing excellent electrical conductivity carbon nanofibers from coal extraction residual. *Clean. Eng. Technol.* **2021**, *4*, 100109. [[CrossRef](#)]
54. Zuo, X.; Xu, P.; Zhang, C.; Li, M.; Jiang, X.; Yue, X. Porous magnetic carbon nanofibers (P-CNF/Fe) for low-frequency electromagnetic wave absorption synthesized by electrospinning. *Ceram. Int.* **2019**, *45*, 4474–4481. [[CrossRef](#)]
55. Zhang, T.; Huang, D.; Yang, Y.; Kang, F.; Gu, J. Fe₃O₄/carbon composite nanofiber absorber with enhanced microwave absorption performance. *Mater. Sci. Eng. B* **2013**, *178*, 1–9. [[CrossRef](#)]
56. Bayat, M.; Yang, H.; Ko, F.K.; Michelson, D.; Mei, A. Electromagnetic interference shielding effectiveness of hybrid multifunctional Fe₃O₄/carbon nanofiber composite. *Polymer* **2014**, *55*, 936–943. [[CrossRef](#)]
57. Yao, F.; Gao, Y.; Chen, F.; Du, Y. Preparation and properties of electrospun peanut protein isolate/poly-L-lactic acid nanofibers. *LWT* **2022**, *153*, 112418. [[CrossRef](#)]
58. Fokin, N.; Grothe, T.; Mamun, A.; Trabelsi, M.; Klöcker, M.; Sabantina, L.; Döpke, C.; Blachowicz, T.; Hütten, A.; Ehrmann, A. Magnetic Properties of Electrospun Magnetic Nanofiber Mats After Stabilization and Carbonization. *Materials* **2020**, *13*, 1552. [[CrossRef](#)] [[PubMed](#)]
59. Weiss, R.; Ehrmann, A. Preliminary report on MFM measurements on magnetic nanofiber mats. *Commun. Dev. Assem. Text. Prod.* **2021**, *2*, 1–7. [[CrossRef](#)]
60. Mamun, A.; Klöcker, M.; Sabantina, L. Needleless Electrospun Magnetic Carbon Nanofiber Mats for Sensor Applications. *Eng. Proc.* **2021**, *6*, 76. [[CrossRef](#)]
61. Bhagwan, J.; Rani, S.; Sivasankaran, V.; Yadav, K.L.; Sharma, Y. Improved energy storage, magnetic and electrical properties of aligned, mesoporous and high aspect ratio nanofibers of spinel-NiMn₂O₄. *Appl. Surf. Sci.* **2017**, *426*, 913–923. [[CrossRef](#)]
62. Yue, C.; Li, M.; Liu, Y.; Fang, Y.; Song, Y.; Xu, M.; Li, J. Three-dimensional printing of cellulose nanofibers reinforced PHB/PCL/Fe₃O₄ magneto-responsive shape memory polymer composites with excellent mechanical properties. *Addit. Manuf.* **2021**, *46*, 102146. [[CrossRef](#)]
63. Pljonkin, A.; Gupta, B.; Rumyantsev, K.; Korovin, I.; Schaefer, G. Features of detection of a single-photon pulse at synchronisation in quantum key distribution systems. In Proceedings of the 6th International Conference on Informatics, Electronics and Vision & 2017 7th International Symposium in Computational Medical and Health Technology (ICIEV-ISCMHT), Himeji, Japan, 1–3 September 2017; pp. 1–5. [[CrossRef](#)]
64. Pljonkin, A.P. Vulnerability of the Synchronization Process in the Quantum Key Distribution System. In *Research Anthology on Advancements in Quantum Technology*, edited by Information Resources Management Association; IGI Global: Hershey, PA, USA, 2021; pp. 345–354. [[CrossRef](#)]
65. Praticò, L.; Fronza, N.; Bartali, R.; Chiappini, A.; Sciubba, E.; González-Aguilar, J.; Crema, L. Radiation propagation in a hierarchical solar volumetric absorber: Results of single-photon avalanche diode measurements and Monte Carlo ray tracing analysis. *Renew. Energy* **2021**, *180*, 482–493. [[CrossRef](#)]
66. Buzhan, P.; Karakash, A.; Teverovskiy, Y. Silicon Photomultiplier and CsI(Tl) scintillator in application to portable H*(10) dosimeter. *Nucl. Instrum. Methods Phys. Res. Sect. A Accel. Spectrometers Detect. Assoc. Equip.* **2018**, *912*, 245–247. [[CrossRef](#)]
67. Barker, C.; Zhu, T.; Rolison, L.; Kiff, S.; Jordan, K.; Enqvist, A. Pulse shape analysis and discrimination for silicon-photomultipliers in helium-4 gas scintillation neutron detector. *EPJ Web Conf.* **2018**, *170*, 07002. [[CrossRef](#)]
68. Bruschini, C.; Homulle, H.; Antolovic, I.M.; Burri, S.; Charbon, E. Single-photon avalanche diode imagers in biophotonics: Review and outlook. *Light Sci. Appl.* **2019**, *8*, 87. [[CrossRef](#)]
69. Prochazka, I.; Blazej, J.; Kodet, J. Effective dark count rate reduction by modified SPAD gating circuit. *Nucl. Instrum. Methods Phys. Res. Sect. A Accel. Spectrometers Detect. Assoc. Equip.* **2015**, *787*, 212–215. [[CrossRef](#)]

70. Meda, A.; Degiovanni, I.; Tosi, A.; Yuan, Z.; Brida, G.; Genovese, M. Quantifying backflash radiation to prevent zero-error attacks in quantum key distribution. *Light Sci. Appl.* **2017**, *6*, e16261. [[CrossRef](#)] [[PubMed](#)]
71. Shields, A. Semiconductor quantum light sources. *Nat. Photon* **2007**, *1*, 215–223. [[CrossRef](#)]
72. Pljonkin, A.; Joshi, S. The Modified Algorithm of Quantum Key Distribution System Synchronization. In *Evolving Technologies for Computing, Communication and Smart World, Lecture Notes in Electrical Engineering*; Singh, P.K., Noor, A., Kolekar, M.H., Tanwar, S., Bhatnagar, R.K., Khanna, S., Eds.; Springer: Singapore, 2021; 694p. [[CrossRef](#)]
73. Pljonkin, A.; Singh, P.K. The Review of the Commercial Quantum Key Distribution System. In Proceedings of the 2018 Fifth International Conference on Parallel, Distributed and Grid Computing (PDGC), Solan, India, 20–22 December 2018; pp. 795–799. [[CrossRef](#)]
74. Bronzi, D.; Villa, F.; Bellisai, S.; Tisa, S.; Tosi, A.; Ripamonti, G.; Zappa, F.; Weyers, S.; Durini, D.; Brockherde, W.; et al. Large-area CMOS SPADs with very low dark counting rate. *Proc. SPIE* **2013**, *8631*, 86311B. [[CrossRef](#)]
75. Hadfield, R. Single-photon detectors for optical quantum information applications. *Nat. Photon* **2009**, *3*, 696–705. [[CrossRef](#)]
76. Buchner, A.; Hadrath, S.; Burkard, R.; Kolb, F.M.; Ruskowski, J.; Ligges, M.; Grabmaier, A. Analytical Evaluation of Signal-to-Noise Ratios for Avalanche and Single-Photon Avalanche Diodes. *Sensors* **2021**, *21*, 2887. [[CrossRef](#)] [[PubMed](#)]
77. Xu, H.; Pancheri, L.; Braga, L.H.C.; Dalla Betta, G.F.; Stoppa, D. Crosstalk Characterization of Single-photon Avalanche Diode (SPAD) Arrays in CMOS 150nm Technology. *Procedia Eng.* **2014**, *87*, 1270–1273. [[CrossRef](#)]
78. Wang, Y.; Jin, X.; Zeng, M.; Peng, Y.; Luo, J. Electric-field-drive single photon avalanche diode with barrier enhancement for fluorescence detection. *Microelectron. J.* **2021**, *115*, 105161. [[CrossRef](#)]
79. Ejdehakosh, S.; Ansarian, M.; Karami, M.A. A new optical random number generator circuit design using single-photon avalanche diodes. *Optik* **2020**, *224*, 165698. [[CrossRef](#)]
80. Lim, K.T.; Kim, H.; Kim, J.; Cho, G. Effect of electric field on primary dark pulses in SPADs for advanced radiation detection applications. *Nucl. Eng. Technol.* **2021**, *53*, 618–625. [[CrossRef](#)]
81. Grothe, T.; Wehlage, D.; Böhm, T.; Remche, A.; Ehrmann, A. Needleless Electrospinning of PAN Nanofibre Mats. *Tekstilec* **2017**, *60*, 290–295. [[CrossRef](#)]
82. Sabantina, L.; Böttjer, R.; Wehlage, D.; Grothe, T.; Klöcker, M.; García Mateos, F.J.; Rodríguez-Mirasol, J.; Cordero, T.; Ehrmann, A. Morphological study of stabilization and carbonization of PAN/TiO₂ nanofiber mats. *J. Eng. Fibers Fabr.* **2019**, *14*, 1558925019862242.
83. Storck, J.L.; Brockhagen, B.; Grothe, T.; Sabantina, L.; Kaltschmidt, B.; Tuvshinbayar, K.; Braun, L.; Tanzli, E.; Hütten, A.; Ehrmann, A. Stabilization and Carbonization of PAN Nanofiber Mats Electrospun on Metal Substrates. *J. Carbon Res.* **2021**, *7*, 12. [[CrossRef](#)]
84. Sabantina, L.; Klöcker, M.; Wortmann, M.; Rodríguez-Mirasol, J.; Cordero, T.; Moritzer, E.; Finsterbusch, K.; Ehrmann, A. Stabilization of polyacrylonitrile nanofiber mats obtained by needleless electrospinning using dimethyl sulfoxide as solvent. *J. Ind. Text.* **2020**, *50*, 224–239. [[CrossRef](#)]
85. Wortmann, M.; Layland, A.S.; Frese, N.; Khamann, U.; Hrothe, T.; Storck, J.L.; Blachowicz, T.; Grzybowski, J.; Husgen, B.; Ehrmann, A. On the reliability of highly magnified micrographs for structural analysis in materials science. *Sci. Rep.* **2020**, *10*, 14708. [[CrossRef](#)]
86. Sabantina, L.; Wehlage, D.; Klöcker, M.; Mamun, A.; Grothe, T.; García-Mateos, F.J.; Rodríguez-Mirasol, J.; Cordero, T.; Finsterbusch, K.; Ehrmann, A. Stabilization of electrospun PAN/gelatin nanofiber mats for carbonization. *J. Nanomater.* **2018**, *2018*, 6131085. [[CrossRef](#)]
87. Wortmann, M.; Frese, N.; Mamun, A.; Trabelsi, M.; Keil, W.; Büker, B.; Javed, A.; Tiemann, M.; Moritzer, E.; Ehrmann, A.; et al. Chemical and Morphological Transition of Poly(acrylonitrile)/Poly(vinylidene Fluoride) Blend Nanofibers during Oxidative Stabilization and Incipient Carbonization. *Nanomaterials* **2020**, *10*, 1210. [[CrossRef](#)] [[PubMed](#)]
88. Gupta, A.K.; Paliwal, D.K.; Bajaj, P. Acrylic Precursors for Carbon Fibers. *JMS Rev. Part C* **1991**, *31*, 1–89. [[CrossRef](#)]
89. Huang, H.D.; Guo, Z.; Yang, P.Y.; Chen, P.; Wu, J. Electrical conductivity and hydrophobicity of graphene oxide-modified carbon nanofibers. *Chem. Phys. Lett.* **2021**, *771*, 138551. [[CrossRef](#)]
90. Liu, C.K.; Feng, Y.; He, H.J.; Zhang, J.; Sun, R.J.; Chen, M.Y. Effect of carbonization temperature on properties of aligned electrospun polyacrylonitrile carbon nanofibers. *Mater. Des.* **2015**, *85*, 483–486. [[CrossRef](#)]
91. Mólнар, K.; Szolnoki, B.; Toldy, A.; Vas, L.M. Thermochemical stabilization and analysis of continuously electrospun nanofibers. *J. Anal. Calorim.* **2014**, *117*, 1123–1135. [[CrossRef](#)]
92. Bashir, Z. A critical review of the stabilisation of polyacrylonitrile. *Carbon* **1991**, *29*, 1081–1090. [[CrossRef](#)]
93. Ismar, E.; Sezai Sarac, A. Oxidation of polyacrylonitrile nanofiber webs as a precursor for carbon nanofiber: Aligned and non-aligned nanofibers. *Polym. Bull.* **2017**, *75*, 485–499. [[CrossRef](#)]